UNIVERSIDADE DE SÃO PAULO

PUBLICAÇÕES

INSTITUTO DE FÍSICA
CAIXA POSTAL 66318
05315-970 SÃO PAULO - SP
BRASIL

NONMODAL ENERGETICS OF RESISTIVE DRIFT WAVES

Suzana J. Camargo
Universidade Estadual Paulista, Campus de Guaratinguetá
Av. Dr. Ariberto Pereira da Cunha, 333
12500-000 Guarantiguetá, SP, Brazil

Michael K. Tippett
Centro de Previsão do Tempo e Estudos Climáticos
Instituto Nacional de Pesquisas Espaciais
Rodovia Presidente Dutra Km 40
12630-000 Cachoeira Paulista, SP, Brazil

Iberê L. Caldas
Instituto de Física, Universidade de São Paulo

Nonmodal energetics of resistive drift waves

Suzana J. Camargo,

Universidade Estadual Paulista, Campus de Guaratinguetá,

Av. Dr. Ariberto Pereira da Cunha, 333,

12500-000, Guaratinguetá, SP, Brazil

Michael K. Tippett,

Centro de Previsão do Tempo e Estudos Climáticos,

Instituto Nacional de Pesquisas Espaciais,

Rodovia Presidente Dutra km 40

12630-000, Cachoeira Paulista, SP, Brazil

Iberê L. Caldas

Instituto de Física, Universidade de São Paulo,

CP: 66318, 05315-970, São Paulo, SP, Brazil

Abstract

The modal and nonmodal linear properties of the Hasegawa-Wakatani system are examined. This linear model for drift-waves in a plasma is nonnormal in the sense of not having a complete set of orthogonal eigenvectors. Nonmodal time-dependent behavior can be important in nonnormal linear systems. The degree of nonnormality of the Hasegawa-Wakatani system depends strongly on the adiabatic parameter and the time scale of interest. On a given time-scale, when the adiabatic parameter is less than a critical value, the drift-waves are dominated by nonmodal effects while for values of the adiabatic parameter greater than the critical value, the behavior is that given by normal mode analysis. The critical adiabatic parameter decreases with time; modal behavior eventually dominates. For small values of the adiabatic parameter and short time scales, the nonmodal growth rates, wave number and phase shifts (between the density and potential fluctuations) are time dependent and differ from those obtained by normal mode analysis.

1 Introduction

A fundamental issue in fluid dynamics is the question of how laminar flows become unstable and eventually turbulent. A method of studying instabilities is to consider the time-evolution of a perturbation of the laminar flow [1]. In general, the evolution of the perturbation is described by a nonlinear system. For small perturbations, the nonlinear system can be approximated by a linear system. When the background flow is time-independent, an eigenmode ("normal mode") analysis of the linear system identifies exponentially growing and decaying perturbations. The dependence of these exponential growth rates on the geometry, the Reynolds number and other parameters allows the theory to make predictions concerning the structure of observed waves of finite amplitude.

Normal mode analysis has been applied to many fluid dynamic stability problems with great success. However, there are some notable cases where the results of normal mode analysis fail to correspond with observed temporal variation and spatial structure of real flows. In particular, normal mode analysis predicts a transition to turbulence for some flows at a much higher Reynolds numbers than that seen in experiment. Attributing this failure to the linearization of a nonlinear problem has led to the development of theories which modify or just eliminate the need for linearization (see e.g. [2, 3]).

Recent studies have shown that for many problems of physical normal mode analysis only gives a partial description of the properties of the linear perturbation equation [4, 5]. When the eigenmodes of the linear system are not orthogonal, or equivalently when the system is *nonnormal*, the solutions of the system may present behavior quite different from that suggested by normal mode analysis. For example, perturbations can be amplified by factors of thousands in nonnormal systems even when all the normal modes of the system are stable [6]. The possibility of amplification of perturbations in nonnormal flows has been known for a long time, but only recently have computational resources made it possible to calculate the magnitudes involved (see [7] and [4] and references therein). Recent applications of nonmodal analysis applied to physical problems are nonmodal growth in in atmospheric flows [8], atmospheric turbulence models [9], stability of the Orr-Sommerfeld [10], models for the transition to turbulence [11], and methods of controling turbulence [12].

In this work, we apply the nonnormal analysis to study the linear properties of a drift-wave turbulence model. The study of instabilities in plasmas is heavily based on normal modes analysis [13] and variational methods such as the *Energy Principle* [14]. Nonlinear stability bounds have been obtained for magnetohydrodynamic flows (see e.g. [15, 16]), though the stability bounds are in general very low. The importance of nonnormality in the stability of plasmas has been studied in a few cases (see e.g. [17, 18]).

Drift-wave turbulence is considered to be a possible cause of anomalous transport in the cool plasma edge region of tokamaks [19]. The Hasegawa-Wakatani model consider here [20, 21] has been extensively studied in bi-dimensional [22, 23, 24] and tri-dimensional numerical simulations [25, 26]. The role of nonlinearity in drft wave models has been examined by comparing the linear behavior given by normal mode analysis with the nonlinear numerical simulation. As a first step in understanding the full nonlinear system, we consider the linearized bi-dimensional Hasegawa-Wakatani equations and study how the nonnormality affects the linear properties of the system.

2 Nonlinear Model

The model of our studies is the Hasegawa-Wakatani system [20, 21]. We consider two-dimensions fluctuations, perpendicular to the static equilibrium magnetic field $\mathbf{B} = B\hat{z}$; magnetic fluctuations are neglected. A nonuniform equilibrium density n_0 with density gradient dn_0/dx in the negative x direction is considered, such that the equilibrium density scale $L_n = n_0/|dn_0/dx|$ is constant. The ions are cold and the electrons are isothermal, $T_i \ll T_e \equiv T$. Therefore, temperature gradients and fluctuations are neglected, as well as finite Larmor effects. We assume that the fluctuation length scales satisfy the usual drift ordering $k_{\parallel} \ll k_{\perp}$. The equations for the time evolution of the density and potential fluctuations are two coupled nonlinear equations given by [20, 21]:

$$\frac{\partial}{\partial t}\nabla_{\perp}^2\phi + (\hat{z} \times \nabla_{\perp}\phi) \cdot \nabla_{\perp}\nabla_{\perp}^2\phi = \mathcal{C}(\phi - n) + \mathcal{D}^{\phi}, \qquad (1)$$

$$\frac{\partial}{\partial t}n + (\hat{z} \times \nabla_{\perp}\phi) \cdot \nabla_{\perp}n + \frac{\partial\phi}{\partial y} = \mathcal{C}(\phi - n) + \mathcal{D}^n, \qquad (2)$$

where the usual dimensionless variables are

$$x \to \frac{x}{\rho_s}, \ y \to \frac{y}{\rho_s}, \ t \to t\frac{c_s}{L_n} \qquad (3)$$

and the normalized potential and density fluctuations are

$$\phi \to \frac{e\phi}{T}\frac{L_n}{\rho_s}, \ n \to \frac{n}{n_0}\frac{L_n}{\rho_s}; \qquad (4)$$

ρ_s is the drift-wave dispersion scale ($\rho_s^2 = c^2 M_i T/(e^2 B^2)$); c_s is the sound speed ($c_s^2 = T/M_i$).

The adiabaticity parameter $\mathcal{C}$, which couples the equations linearly and determines the character of the system is defined as [22, 23]

$$\mathcal{C} = \frac{T}{n_0 e^2 B^2}\frac{k_\parallel^2}{c_s/L_n}. \qquad (5)$$

In the limit $\mathcal{C} \gg 1$, the electron response is almost adiabatic, meaning that the fluctuations of the density follow very nearly the fluctuations of the potential. In this limit, Eqs. (1) and (2) reduce to the Hasegawa-Mima equation [27]. In the opposite limit, $\mathcal{C} \ll 1$, Eq. (1) reduces to the Navier-Stokes equation, by which density fluctuations are passively advected.

The viscous and diffusive dissipation terms $\mathcal{D}^\phi$ and $\mathcal{D}^n$, respectively, are chosen to have the form

$$\mathcal{D}^\phi = \nu\nabla_\perp^6\phi, \ \mathcal{D}^n = \nu\nabla_\perp^4 n, \qquad (6)$$

in order to confine the dissipation to the smallest scales resolved in the system. The Hasegawa-Wakatani system is a simple model for drift-wave turbulence in a collisional plasma with a magnetic field without shear. It is an autonomous system describing the excitation and damping of modes in terms of a few collisional parameters, leading to a stationary level of turbulence without need of external forcing [22].

We usually choose times in our study of the order $t = 10$, $t = 50$, $t = 100$, as we want to compare our work with previous numerical simulations of the bi-dimensional Hasegawa-Wakatani system [22]. In these numerical simulations, there are two phases, a linear phase followed by a nonlinear phase with a stationary turbulent regime.

3 Linear Model

To study the linear properties of the system of equations (1) and (2), we neglect the nonlinear terms and expand ϕ and n in a double Fourier series in x and y. For any wave number pair $\mathbf{k} = (k_x, k_y)$ the time evolution of the Fourier components of ϕ and n have the form

$$\frac{d}{dt}\mathbf{u_k} = \mathbf{A_k}\mathbf{u_k}, \qquad (7)$$

where

$$\mathbf{u_k} = \begin{pmatrix} \phi_\mathbf{k} \\ n_\mathbf{k} \end{pmatrix}, \qquad (8)$$

$$\mathbf{A_k} = \begin{pmatrix} -\mathcal{C}/k^2 - \nu_\phi k^4 & \mathcal{C}/k^2 \\ -ik_y + \mathcal{C} & -\mathcal{C} - \nu_n k^4 \end{pmatrix}, \qquad (9)$$

$$k = \sqrt{k_x^2 + k_y^2}. \qquad (10)$$

There is no coupling between distinct pairs of wavenumbers. This property reduces greatly the numerical cost of analyzing the problem.

Assuming that the time-dependence of the perturbations is exponential, e.g. $\sim e^{\gamma t}$, reduces Eq. 7 to the eigenvalue problem

$$(\gamma\mathbf{I} - \mathbf{A})\mathbf{u} = 0, \qquad (11)$$

where $\mathbf{u}$ is the vector containing all the Fourier component $\mathbf{u_k}$ and $\mathbf{A}$ is the block-diagonal matrix with entries $\mathbf{A_k}$; if the number of modes in k_x and k_y is N then $\mathbf{u}$ is a vector of length $2N^2$ and $\mathbf{A}$ is a $2N^2 \times 2N^2$ matrix. Equation (11) has a nonzero solution only if γ is an eigenvalue of $\mathbf{A}$. The normal mode growth rate β_0 is calculated by finding the eigenvalue of $\mathbf{A}$ with the largest real part. The linearized Hasegawa-Wakatani equations have been studied using such normal mode analysis (see e.g. [22]). However, an analysis of the linear system including time-dependent, nonmodal behavior, or an analysis of the *approximate* solutions of (11) has not been done yet, as far as we know. Therefore, a distinguishing feature of this analysis is that we do not take an exponential time-dependence.

The range of behavior possible in this model and the need to account for both modal and nonmodal behavior can be seen by considering two extreme limiting values of $\mathcal{C}$. First,

for $\mathcal{C} \gg 1$, neglecting all terms that do not contain $\mathcal{C}$ gives

$$\frac{d}{dt}\left(\phi_{\mathbf{k}} + \frac{n_{\mathbf{k}}^2}{k_\perp^2}\right) = 0 \tag{12}$$

and

$$\frac{d}{dt}\left(\phi_{\mathbf{k}} - \frac{n_{\mathbf{k}}^2}{k_\perp^2}\right) = \frac{2\mathcal{C}}{k_\perp^2}\left(\phi_{\mathbf{k}} - \frac{n_{\mathbf{k}}^2}{k_\perp^2}\right), \tag{13}$$

the adiabatic limit with pure exponential growth. The other extreme $\mathcal{C} = 0$ gives $\phi_{\mathbf{k}} = const.$ and $n_{\mathbf{k}} = -ik_y t \phi_{\mathbf{k}} + const.$, nonmodal algebraic growth. For intermediate values of $\mathcal{C}$ we expect to see a mixture of modal and nonmodal behavior.

The fundamental reason that (7) may present behavior different from that suggested by the eigenvalue problem of (11) is that the matrix $\mathbf{A}$ is *nonnormal*. That is to say, it does not have a complete set of orthogonal eigenvectors or equivalently it does not commute with its adjoint. Since both the notion of orthogonality and adjoint depend on the choice of inner product, it is necessary to use an inner product coming from a physically relevant norm. The most obvious choice of norm $\| \cdot \|$ is that coming from the total energy of the fluctuations E given by

$$E = \frac{1}{2}\int d^2x \left(|\nabla_\perp^2 \phi|^2 + n^2\right) = \frac{1}{2}\sum_{\mathbf{k}} \left(k^2 \phi_{\mathbf{k}}^2 + n_{\mathbf{k}}^2\right), \tag{14}$$

an invariant of the purely nonlinear Hasegawa-Wakatani system [22]. It is a direct calculation to verify that the dynamical operator $\mathbf{A}$, which describes the linear evolution of the Hasegawa-Wakatani system is a *nonnormal* operator with respect to the energy norm.

The basic quantities used in our investigation of the linear Hasegawa-Wakatani system are the ratio ξ of the energy of the fluctuations at time t to the initial energy of the fluctuations defined by

$$\xi(t) = \frac{\|\mathbf{u}(t)\|}{\|\mathbf{u}(0)\|}, \tag{15}$$

and the growth rate $\beta(t)$ defined by $\beta = t^{-1}\ln\xi$. The ratio $\xi(t)$ depends on the initial energy of the fluctuations $\mathbf{u}(0)$ and time. We shall examine the energy growth ratio $\xi(t)$ for several choices of initial conditions using subscripts to distinguish the various choices. We use the

7

notation $\xi_0(t)$ to indicate that $\mathbf{u}_0$ is taken to be the eigenvector of $\mathbf{A}$ whose real part is β_0. Then

$$\xi_0(t) = e^{\beta_0 t}. \tag{16}$$

Note that $\beta_0 = t^{-1}\ln\xi_0(t)$ is the normal mode growth rate and is constant in time. We use the notation $\xi_1(t)$ for the case where $\mathbf{u}(0)$ is chosen such that ξ is maximized, i.e.

$$\xi_1(t) = \max_{\mathbf{u}(0)} \frac{\|\mathbf{u}(t)\|}{\|\mathbf{u}(0)\|}. \tag{17}$$

The quantity $\xi_1(t)$ is related to $\mathbf{A}$ by $\xi_1(t) = \|e^{\mathbf{A}t}\|$. If $\mathbf{A}$ is normal, $\xi_1(t) = \xi_0(t)$ for all time. More generally, $\xi_1(t) \geq \xi_0(t)$ though in the limit of large time [29]

$$\lim_{t\to\infty} \beta_1(t) = \beta_0. \tag{18}$$

It is important to note that when the growth is nonmodal, the initial value of the fluctuations that produces the maximum growth at a particular time will not necessarily be the initial value that produces the maximum growth at any other time. Therefore, to see the behavior of a single choice of initial fluctuation value, we define the following energy growth ratios: $\xi_2(t)$–the initial condition is chosen to produce maximum growth in the limit of large time, $\xi_3(t)$–the initial condition is chosen to produce maximum growth at a specified finite time τ, and $\xi_4(t)$–the initial condition is chosen to produce maximum growth in the limit of small time. Recall again that for normal systems all these growth ratios coincide. The final measure of the energy growth $\xi_5(t)$ is obtained by considering the expected time-evolution of random initial conditions. Details of the calculation of these ratios are given in the Appendix.

In Section 4 we investigate the various energy growth ratios and examine how they depend on $\mathcal{C}$ and on the time-scale. We performed some tests with our calculations and concluded that our results are not dependent on the number of modes, when a reasonable number of modes is considered. We choose in most of our calculations the number of modes $N = 32$, as when this number is increased, there are not any further changes in our results. The value taken for the dissipation is in most cases $\nu = 10^{-5}$, which is the order of magnitude of considered in numerical simulations [22].

8

4 Results

4.1 Spectra and Pseudospectra

In this section the transient growth properties of the dynamics are shown to be connected to the *pseudospectrum* of $\mathbf{A}$. The set of eigenvalues or *spectrum* of a matrix $\mathbf{A}$ is the set $\Lambda(\mathbf{A})$ of complex numbers z such that $(z\mathbf{I} - \mathbf{A})$ is singular. In Fig. 1(b)-(d), we show the spectra (in black), for $\mathcal{C} = 10^{-5}$, $\mathcal{C} = 10^{-3}$ and $\mathcal{C} = 1$. The values of the modal growth rate β_0 can be simply read from these plots. The modal growth rate has a strong dependence on $\mathcal{C}$, as already noted in [22]; the values of the spectra and the form of the spectra change with $\mathcal{C}$. The *pseudospectrum* of a nonnormal matrix may provide more information than its spectrum [10, 30]. The pseudospectrum is defined as follows. The complex number z is in the ϵ-pseudospectrum $\Lambda_\epsilon(\mathbf{A})$ if $z \in \Lambda(\mathbf{A} + \mathbf{E})$ for $\|\mathbf{E}\| \leq \epsilon$. Note that $\Lambda_0(\mathbf{A}) = \Lambda(\mathbf{A})$. If $z \in \Lambda_\epsilon(\mathbf{A})$ then it is in some sense an approximate eigenvalue, in that, there is some vector $\mathbf{u}$ such that $\|\mathbf{A}\mathbf{u} - z\mathbf{u}\| \leq \epsilon$.

Analysis of the pseudospectrum gives stronger conditions on energy growth than does the spectrum. Roughly speaking, the energy growth depends on how far the pseudospectrum of $\mathbf{A}$ extends into the right half-plane. This idea is made explicit by defining the extension $\alpha(\epsilon)$ of the pseudospectrum into the right half-plane by

$$\alpha(\epsilon) = \max_{z \in \Lambda_\epsilon(\mathbf{A})} \operatorname{Re} z. \tag{19}$$

Note that $\alpha(0) = \beta_0$ is the growth rate given by the normal mode analysis. It can be shown that [10]

$$\max_{t \geq 0} \|e^{\mathbf{A}t}\| \geq \max_{\epsilon > 0} \frac{\alpha(\epsilon) - \alpha(0)}{\epsilon} e^{\beta_0 t}. \tag{20}$$

Hence, if $(\alpha(\epsilon) - \alpha(0))/\epsilon > 1$ there are fluctuations that grow more than predicted by normal mode analysis.

The calculation of the ϵ-pseudospectra is computationally expensive. An estimate of $\Lambda_\epsilon(\mathbf{A})$ can be obtained relatively inexpensively using a Monte Carlo approach. The eigenvalues of $(\mathbf{A} + \mathbf{E})$ are calculated where $\|\mathbf{E}\| = \epsilon$ and $\mathbf{E}$ is a random complex matrix whose entries are independently distributed Gaussian random variables with mean zero and unit
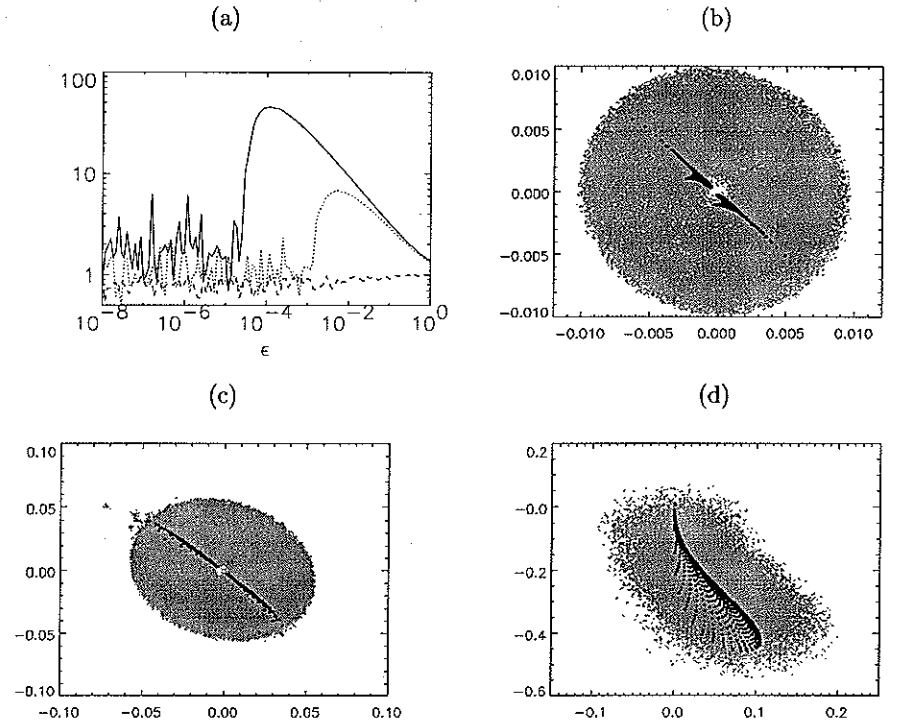

Figure 1: (a) The quantity $(\alpha(\epsilon) - \alpha(0))/\epsilon$ plotted as a function of ϵ for $\mathcal{C} = 10^{-5}$ (solid-line), $\mathcal{C} = 10^{-3}$ (dotted-line) and $\mathcal{C} = 1$ (dashed line). The spectrum $\Lambda(\mathbf{A})$ (black) and ϵ-pseudospectrum $\Lambda_\epsilon(\mathbf{A})$ (gray) for (b) $\mathcal{C} = 10^{-5}$ and $\epsilon = 10^{-4}$ (c) $\mathcal{C} = 10^{-3}$ and $\epsilon = 3.2 \times 10^{-3}$ and (d) $\mathcal{C} = 1$ and $\epsilon = 10^{-1}$. Panel (d) shows only the most unstable branch of the spectrum.

variance. Repeating this procedure for many realizations of **E** gives an estimate of $\Lambda_\epsilon(\mathbf{A})$. Figures 1(b) – (d) show Monte Carlo estimates of the pseudospectrum (in gray) using 10 realizations for particular values of ϵ. In Fig. 1(a) the quantity $(\alpha(\epsilon) - \alpha(0))/\epsilon$ estimated by the Monte Carlo method using 50 realizations is plotted. Figure 1(a) shows that the cases $\mathcal{C} = 10^{-5}$ and $\mathcal{C} = 10^{-3}$ produce transient growth that is a factor of respectively 45 and 6.8 greater than the normal mode exponential growth (see (20)). For $\mathcal{C} = 1$, $(\alpha(\epsilon) - \alpha(0))/\epsilon \approx 1$, the same as for a normal matrix. This result combined with the previous remarks shows that for the case $\mathcal{C} = 1$, the pseudospectrum does not predict energy growth greater than that given by normal mode analysis.

For the cases $\mathcal{C} = 10^{-5}$ and $\mathcal{C} = 10^{-3}$, the quantity $(\alpha(\epsilon) - \alpha(0))/\epsilon \approx \mathcal{O}\left(\epsilon^{-p}\right)$ for values of ϵ that are not too small ($10^{-4} \leq \epsilon \leq 1$) with $p = 0.35$ and $p = 0.40$ respectively. Such non-analytic (fractional power) dependence of the eigenvalues on perturbation size is typical of nonnormal matrices[31]. For very small values of ϵ, the behavior is more complex. A reason for there being two types of behavior is that the most sensitive eigenvalues (large $(\alpha(\epsilon) - \alpha(0))/\epsilon$) are not the most unstable eigenvalues ($\alpha(0) = \beta_0$ large). For relatively large ϵ, perturbations to the most sensitive eigenvalues of **A** dominate the calculation of $\alpha(\epsilon)$. However, if the highly sensitive eigenvalues are not the most unstable ones, then for small enough values of ϵ, $(\alpha(\epsilon) - \alpha(0))/\epsilon$ will reflect the properties of the most unstable eigenvalues, i.e. those closest to $\alpha(0)$. Numerical calculations (not shown here) support this explanation. The relevant consequence of this point is that enhanced nonmodal growth is due to a different part of the spectrum (different wave numbers) than that which produces maximum modal growth.

4.2 Energy growth ratios

We now examine in detail the various energy growth ratios. Figure 2 shows the time evolution of the energy growth ratios $\xi_{\{0-5\}}(t)$ for $\mathcal{C} = 10^{-5}, 10^{-3}, 0.1, 1.0$. First, we discuss some features of the modal growth $\xi_0(t)$ and maximum growth $\xi_1(t)$ curves. For large time the relation $\beta_1(t) = \beta_0$ must hold, i.e. $\xi_0(t)$ and $\xi_1(t)$ must be parallel. The time required for $\beta_1(t)$ to approximate β_0 depends on the adiabaticity parameter $\mathcal{C}$; for large $\mathcal{C}$ (0.1 and 1.0), $\xi_0(t)$ and $\xi_1(t)$ are virtually indistinguishable for all values of t. Figs. 2(a) and 2(b) show

that for $t < 50$ and small $\mathcal{C}$, $\beta_1(t)$ and $\beta_0(t)$ are quite different. For the case of $\mathcal{C} = 10^{-5}$, $\xi_0(t)$ and $\xi_1(t)$ are still not parallel at $t = 100$; for $\mathcal{C} = 10^{-3}$, the energy ratio growth rate relaxes to the modal one at about $t = 50$. The increased nonmodal small-time growth causes the difference between the curves $\xi_1(t)$ and $\xi_0(t)$ at $t = 100$ to be $\mathcal{O}(100)$ and $\mathcal{O}(10)$ for $\mathcal{C} = 10^{-5}$ and $\mathcal{C} = 0.1$ respectively. We note that the lower bounds obtained from the pseudospectra and (20) are satisfied.

The energy growth ratio curve $\xi_2(t)$ shows the time evolution of the energy of fluctuations whose initial values are chosen so that ξ coincides with $\xi_1(t)$ for large time. As shown in the Appendix, the wave number **k** of these fluctuations is the same as that of the modal instability. However, the partitioning of ϕ_k and n_k is such that enhanced (compared to modal) growth is achieved [32]. In general, the limit $\xi_2(t) \rightarrow \xi_1(t)$ is satisfied only in the limit of large time. However, for this system, only for the case $\mathcal{C} = 10^{-3}$ is there visible difference between the $\xi_2(t)$ and $\xi_1(t)$ curves. An explanation for this behavior is that for $\mathcal{C} = 10^{-3}$ the wave number of the modal instability presents relatively weak nonmodal instability while in the other cases, the wave number of the modal instability also presents a strong nonmodal instability. In the next section we examine in more detail the wave number dependence and confirm this explanation (see Fig. 3(b)). The energy growth ratio $\xi_3(t)$ shows the time evolution of fluctuations whose initial value are chosen so that $\xi_3(\tau) = \xi_1(\tau)$ for $\tau = 100/3$. For the case $\mathcal{C} = 10^{-3}$ and for $t > 50$, $\xi_3(t)$ grows with a rate less than the maximum modal growth rate, indicating in this case that the wavenumber leading to maximal finite time growth is different from the wavenumber at which the maximal modal growth occurs. Only for the case $\mathcal{C} = 10^{-3}$ is there visible difference between the $\xi_1(t)$ and $\xi_3(t)$ curves for the same reasons mentioned above.

The curve $\xi_4(t)$ shows the evolution of fluctuations with maximum initial growth, i.e., $\xi_4(t)$ is tangent to $\xi_1(t)$ at $t = 0$. Maximum initial growth does not lead to long time maximum growth. In all the cases, $\xi_4(t)$ eventually grows at a rate less than the modal growth rate β_0. This behavior implies that for all the values of $\mathcal{C}$ considered, the normal modal analysis does not identify the wave numbers which present maximum short-time nonmodal growth. For the case $\mathcal{C} = 10^{-5}$ the growth of $\xi_4(t)$ is not too much less than $\xi_1(t)$. Later we show that this is due to the relatively weak dependence of the nonmodal growth

rate on the wavenumber.

A curve of special interest is that of $\xi_5(t)$, which to corresponds the time evolution of the expected energy for random initial conditions. Intuitively, this would seem to be a reasonable model of what happens in experiments; all the modes are excited, rather than one particular mode. Looking at Fig. 2, we note that for small values of C and small time, ξ_5 follows well the ξ_1 curve. This behavior suggests that for these values of C and time-scales, nonmodal growth is not isolated to a few wavenumbers but is a broad-spectrum phenomena, as will be confirmed later. Eventually, $\xi_5(t)$ must be parallel to ξ_0 as modal behavior dominates. In general, ξ_5 will be less than ξ_0 since the ensemble average is over all wave numbers and modal instability is found only at a few wave numbers. Fig. 2(b) shows quite clearly the transition of ξ_5 from nonmodal dominant to modal dominant behavior (not shown here but eventually $\xi_5(t)$ is indeed parallel to $\xi_0(t)$). Figures 2(c) and 2(d) for $C = 0.1$ and $C = 1$ respectively show that without broad-spectrum initial nonmodal growth, the expected energy of the random initial condition requires some time before the effects of the modal instability begin to be seen. This phenomena of random initial conditions requiring time to "organize" before growing is well-known in the meteorological community and has generated several techniques to calculate "optimal" random initial conditions for ensemble forecasting [33, 34]. Again in this case as the modal instabilities are confined to a few wavenumbers and the average is over all wave numbers ξ_5 is less than ξ_1.

In summary, the general features are that for small values of C the normal mode growth rate and associated time-scale do not give a complete picture of the linear system; nonmodal growth rates is larger than modal growth. Second, in all cases the normal mode analysis does not identify the wave number at which maximum initial growth occurs. Third, examining the response to random initial conditions shows that the nonmodal behavior is robust for the small C case and that for large C the damped modes present lengthen the time it takes for the system to produce modal growth.

An important point is that for $C = 10^{-5}$, the modal growth is small, suggesting a long time scale, but the nonmodal growth is in reality much faster, as can be seen by the length of the nonmodal phase (compare ξ_0 and ξ_1 in Fig. 2(a)). This was already observed when we studied the turbulent system, while for small C a saturated turbulent state was reached
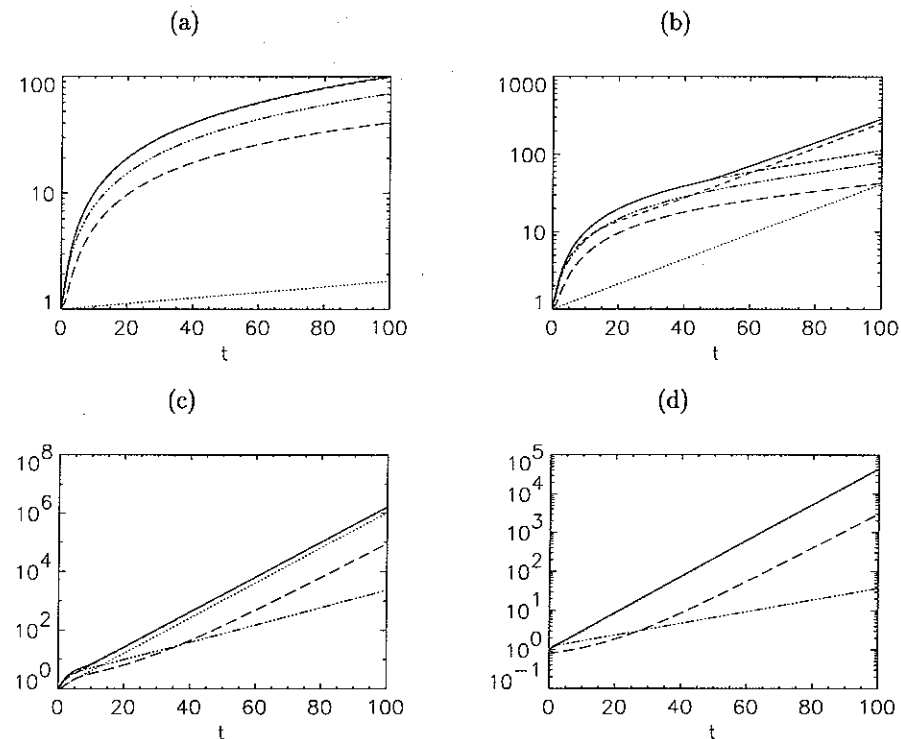
Figure 2: Time evolution of the norms $\xi_{\{0-5\}}(t)$ (dotted, solid, dash-dot, dash-dot-dot-dot, and dash) for (a) $C = 10^{-5}$, (b) $C = 10^{-3}$, (c) $C = 0.1$, and (d) $C = 1$.

rather fast, it took a long time to reach a saturated state for large values of $\mathcal{C}$ [22]. Therefore, the nonnormality can have a strong influence in the linear phase of a turbulent system.

4.3 Growth rates

A number of the features seen in the energy growth ratio curves of the previous section can only be explained by a more detailed examination of the wave number dependence of the growth rates β. In Figure 3 we show $\beta_1(t)$ ($t = 10$, $t = 50$ and $t = 100$) and β_0 as functions of k_y for $k_x \equiv 0$ and $\mathcal{C} = 10^{-5}$, $\mathcal{C} = 10^{-3}$, $\mathcal{C} = 0.1$ and $\mathcal{C} = 1$. The magnitude of the finite time growth rates for small $\mathcal{C}$ and $t = 10$ are slightly larger than those for $\mathcal{C} = 0.1$ (approximately the $\mathcal{C}$ that gives the maximum modal growth rate). This dependence on $\mathcal{C}$ is exactly the opposite of that seen in the modal growth rate which is a decreasing function of $\mathcal{C}$. As the time t increases, the limit $\beta_1(t) \to \beta_0$ must hold. The rate of convergence of $\beta_1(\tau)$ to β_0 depends on $\mathcal{C}$. For small $\mathcal{C}$ the convergence is slow; for $\mathcal{C} = 10^{-5}$ and $\mathcal{C} = 10^{-3}$ the $\beta(t = 100)$ and β_0 curves are quite distinct. As $\mathcal{C}$ increases, the time scale for convergence becomes smaller. Also for large $\mathcal{C}$, the convergence is nonuniform in k_y; $\beta_1(t) \to \beta_0$ first for small values of k_y.

The fact that the modes corresponding to large k_y are in reality growing (i.e. are not damped) for small values of $\mathcal{C}$ even as larger times are considered (see Fig. 3(a)) may be significant in nonlinear numerical simulations of drift-wave turbulence where there is coupling between modes. If these modes were damped a certain spatial resolution would be enough to study that case, however if these modes are in reality growing, the spatial resolution will not be enough and this could influence the results of the numerical simulations.

In Figure 4 we compare β_0 and β_1 as functions of time for two values of $\mathcal{C}$, $\mathcal{C} = 10^{-5}$ and $\mathcal{C} = 0.1$. The influence of the parameter $\mathcal{C}$ on the modal growth rate β_0 is very strong. However, for small time ($t < 20$) the nonmodal growth rates for the two cases are comparable; in both cases there is enhanced nonmodal growth. We repeat this calculation in Fig. 5, to compare the effect of two values of ν on the growth rates β_0 and β_1. We notice that for $\mathcal{C} = 10^{-5}$ (Fig. 5(a)) the difference of the growth rates β_0 and β_1 for $\nu = 10^{-5}$ and $\nu = 0.1$ is very small. By comparison, for $\mathcal{C} = 0.1$ the difference of the growth rates for these two different values of ν is bigger, especially for smaller times. Therefore, we can conclude that
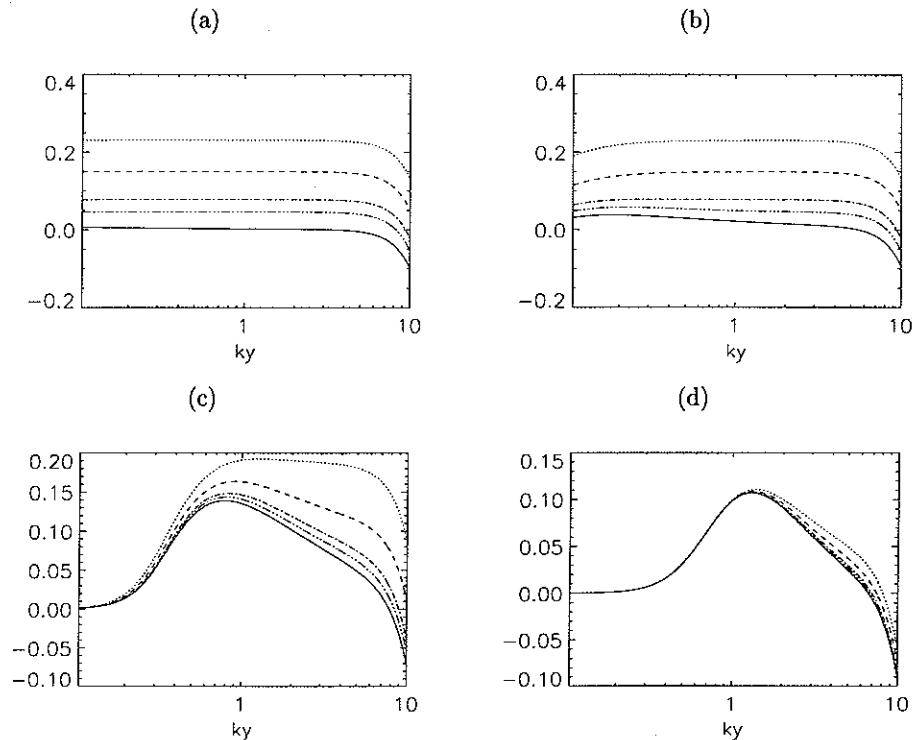
Figure 3: The growth rates $\beta_1(t)$ ($t = 10$ (dotted); $t = 20$ (dashed); $t = 50$(dashed-dot); $t = 100$ (dash-dot-dot-dot)) and β_0 (solid) as functions of k_y for (a) $\mathcal{C} = 10^{-5}$, (b) $\mathcal{C} = 10^{-3}$, (c) $\mathcal{C} = 0.1$ and (d) $\mathcal{C} = 1$.
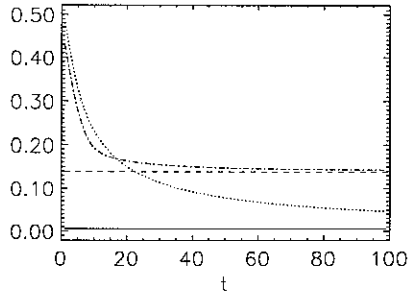
Figure 4: Growth rate $\beta_1(t)$ and grow rate β_0, for $\mathcal{C} = 10^{-5}$ (dotted; solid) and $\mathcal{C} = 0.1$ (dot-dash; dashed).

the influence of dissipation is more important in the adiabatic regime (bigger values of $\mathcal{C}$) and for smaller times. This role of viscosity is to be expected since for small $\mathcal{C}$ the the modal and nonmodally unstable wave lengths are long and while for for large $\mathcal{C}$ they are small (see Fig. 3).

In Figure 6(a) we show the growth rates β_0 and $\beta_1(t)$ ($t = 10$, $t = 20$, $t = 50$ and $t = 100$) as functions of $\mathcal{C}$. For large values of $\mathcal{C}$ ($\mathcal{C} > 1$) β_0 and β_1 coincide for all values of t. For small values of $\mathcal{C}$, β_0 differs greatly from $\beta_1(t)$. For small enough $\mathcal{C}$, $\beta_1(t)$ does not depend on $\mathcal{C}$ and the $\mathcal{C} = 0$ result of pure algebraic growth $\sim k_y t$ is recovered. Figure 6(b) shows the wavenumbers corresponding to the growth rates in Fig. 6(a) as a function of $\mathcal{C}$. We denote by $k_0^{\max}$ and $k_1^{\max}(t)$ the perpendicular wave number corresponding to the growth rates β_0 and $\beta_1(t)$ ($t = 10$, $t = 20$, $t = 50$ and $t = 100$). The behavior we see is the following. At a particular time t, $k_1^{\max}(t) \approx k_0^{\max}$ for values of the adiabatic parameter $\mathcal{C}$ above some cut-off $\mathcal{C}_{\text{crit}}(t)$. For $\mathcal{C} < \mathcal{C}_{\text{crit}}(t)$, $k_1^{\max}(t) \approx k_1^{\max}(10)$. For values of $\mathcal{C}$ near the cut-off there is transition conecting the modal and nonmodal behavior. The cut-off value $\mathcal{C}_{\text{crit}}(t)$ is a decreasing function of time.
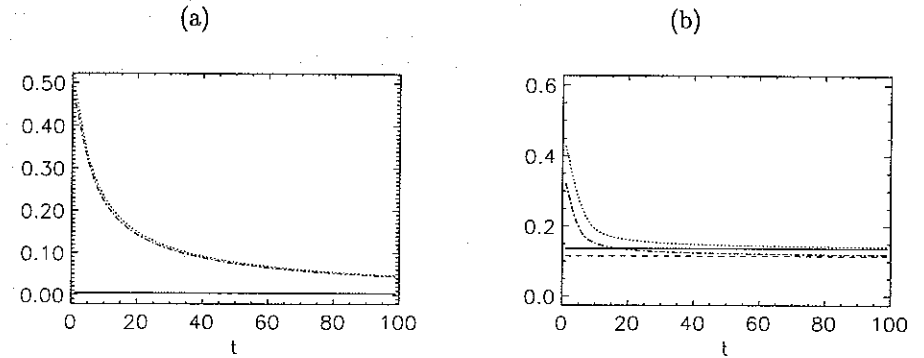

Figure 5: The growth rates $\beta_1(t)$ and β_0 plotted as functions of time for $\nu = 10^{-5}$ (dotted; solid) and $\nu = 10^{-1}$ (dot-dashed; dashed) with (a) $\mathcal{C} = 10^{-5}$ and (b) $\mathcal{C} = 0.1$.
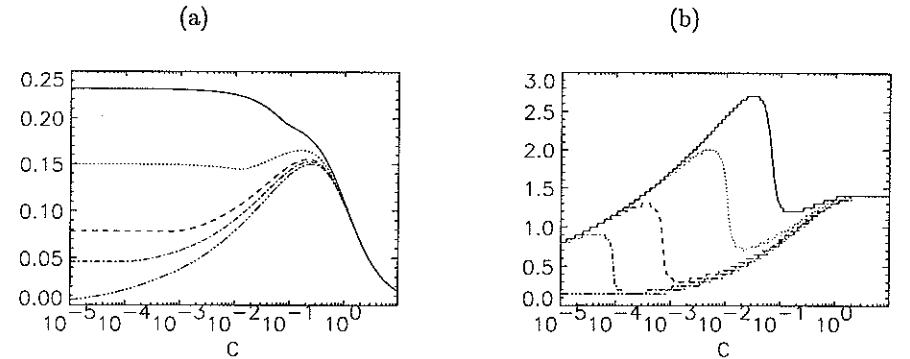

Figure 6: (a) The growth rates β_0 (dot-dot-dot-dash) and $\beta_1(t)$ for $t = 10$ (solid), $t = 20$ (dotted), $t = 50$ (dashed) and $t = 100$ (dot-dash) plotted as functions of $\mathcal{C}$. (b) Values of k_0^{max} and $k_1^{max}(t)$ for the same values of t (and line styles) plotted as a function of $\mathcal{C}$.

4.4 Phase shifts

A quantity of interest for transport studies is the the phase shift $\delta_{\mathbf{k}}$ between $n_{\mathbf{k}}$ and $\phi_{\mathbf{k}}$ defined by

$$\delta_{\mathbf{k}} = \mathrm{Im}\log n_{\mathbf{k}}^{\dagger}\phi_{\mathbf{k}}. \tag{21}$$

In nonlinear numerical simulations, the phase-shift has been calculated by averaging (21) over realizations or in time. A normal mode linear phase-shift $\delta_{\mathbf{k}}^{0}$ is calculated by taking $n_{\mathbf{k}}$ and $\phi_{\mathbf{k}}$ to be the components of the modal instability with wave number $\mathbf{k}$. In analogy, a nonmodal finite-time phase shift $\delta_{\mathbf{k}}^{1}(t)$ can be calculated by using the components of the nonmodal instability with wave number $\mathbf{k}$. In Fig. 7, we compare the linear phase-shifts $\delta_{\mathbf{k}}^{0}$ and $\delta_{\mathbf{k}}^{1}(t)$ for $k_x = 0$ for various values of $\mathcal{C}$ and t. For all values of $\mathcal{C}$ considered (Figs.7(a) - 7(d)) the nonmodal phase-shift is initially larger than the modal one and for larger times they tend to have the same values. The larger the value of $\mathcal{C}$ the faster this agreement is reached; for $\mathcal{C} = 1$ (Fig.7(d)) both phase-shifts already coincide for all values of k_y at $t = 10$. In contrast, for $\mathcal{C} = 10^{-5}$ (Fig.7(a)) the phase-shifts still differ at a time $t = 100$. The nonmodal phase-shift first agrees with the modal phase-shift for small values of k_y and this agreement reaches larger values of k_y for longer times.

The linear phase-shift $\delta_{\mathbf{k}}^{5}(t)$ found by calculating the expected value of $\mathrm{Im}\log n_{\mathbf{k}}^{\dagger}\phi_{\mathbf{k}}$ is shown in Fig. 8; $\delta_{\mathbf{k}}^{5}(t)$ is calculated in the same fashion as $\xi_{5}(t)$. In the limit of large time $\delta_{\mathbf{k}}^{5}(t)$ also goes to the normal mode linear phase-shift as does $\delta_{\mathbf{k}}^{1}(t)$ (see Fig. 7). The finite time values $\delta_{\mathbf{k}}^{5}(t)$ are quite different from those calculated in Fig. 7 for small values of $\mathcal{C}$ and small wave numbers k_y. $\delta_{\mathbf{k}}^{1}(t)$ and $\delta_{\mathbf{k}}^{5}(t)$ only differ for $\mathcal{C} = 10^{-5}$ and $\mathcal{C} = 10^{-3}$ and for wave numbers $k_y < 0.1$. In these cases $\delta_{\mathbf{k}}^{5}(t)$ is smaller than the normal mode linear phase-shift, while $\delta_{\mathbf{k}}^{1}(t)$ is larger than the later. For $\mathcal{C} = 0.1$ time-dependence is seen only for short times and large wave numbers. For $\mathcal{C} = 1$ the phase shift is time-independent for the time-scales shown.

The phase-shifts obtained here can be compared for $\mathcal{C} = 0.1$ and $\mathcal{C} = 1$ with the nonlinear phase-shifts calculated in nonlinear numerical simulation [22]. The linear and nonlinear phase-shifts are very different for $\mathcal{C} = 0.1$; in this case, the nonlinear phase-shift is strongest at low k and drops towards zero elsewhere, a tendency that is thought to be due to the
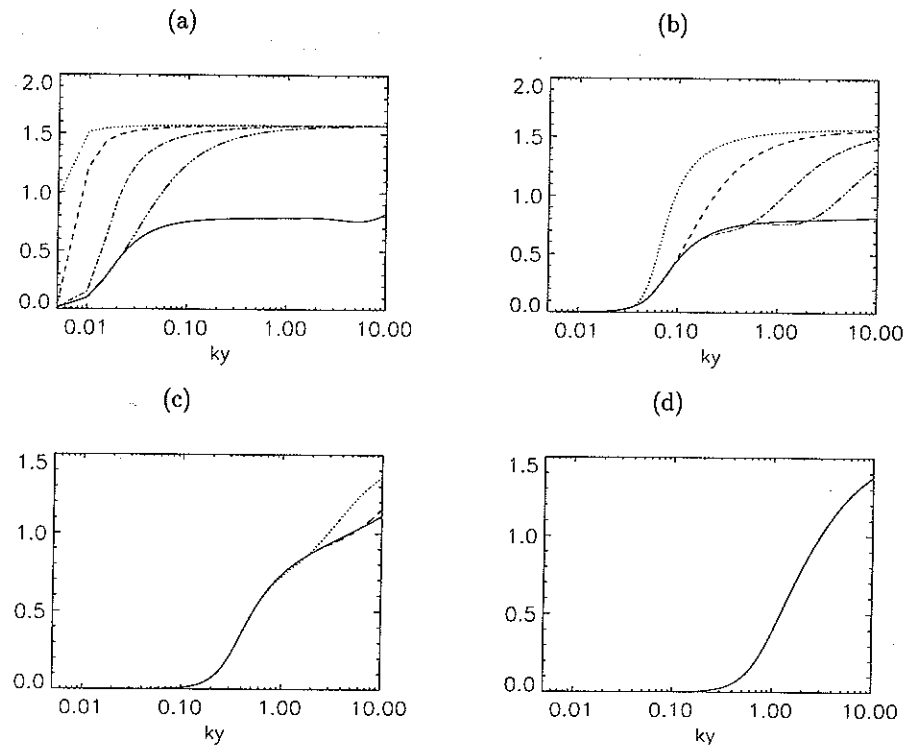
Figure 7: Normal mode linear phase shift $\delta_{\mathbf{k}}^{0}$ and nonmodal linear phase shift $\delta_{\mathbf{k}}^{1}(t)$ ($t = 10$, $t = 20$, $t = 50$, and $t = 100$) as a functions of k_y for (a) $\mathcal{C} = 10^{-5}$, (b) $\mathcal{C} = 10^{-3}$ (c) $\mathcal{C} = 0.1$ and (d) $\mathcal{C} = 1$. Here $\rho_s = 0.005$, $N = 2000$ and $k_x = 0$.

(a)

(b)

(c)

(d)

Figure 8: Ensemble averaged linear phase shift $\delta_k^5(t)$ ($t = 10$, $t = 20$, $t = 50$, and $t = 100$) as a functions of k_y for (a) $C = 10^{-5}$, (b) $C = 10^{-3}$ (c) $C = 0.1$ and (d) $C = 1$. Here $\rho_s = 0.005$, $N = 2000$ and $k_x = 0$.
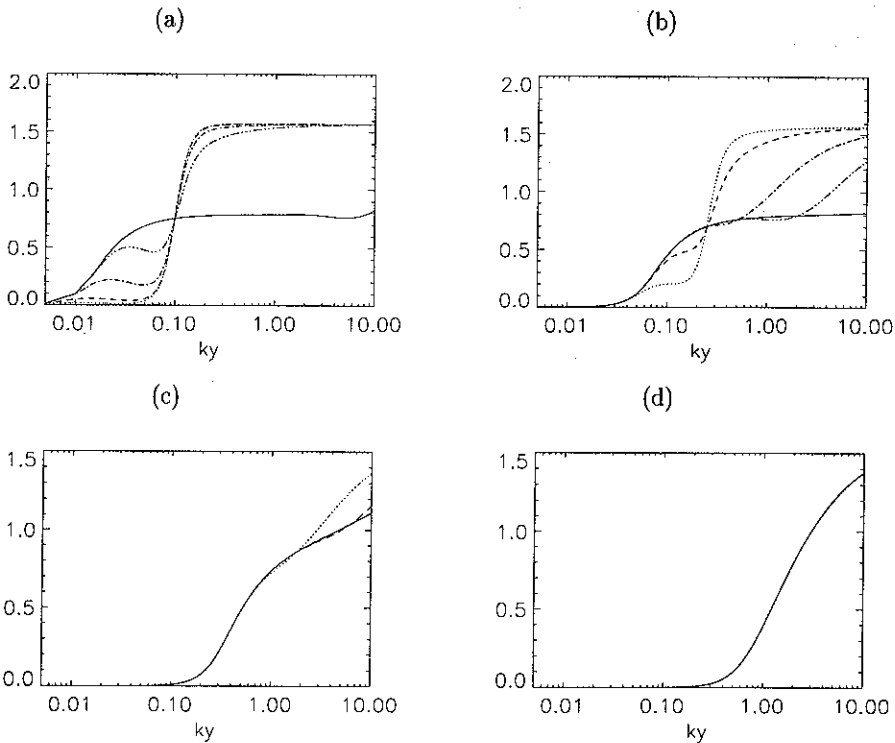
turbulent advection, which tends to randomize the relationship between n and ϕ. For $C = 1$ the nonlinear and linear phase-shifts have the same dependence on k, though the nonlinear phase-shift is still lower than the linear ones.

5 Conclusions

We have examined the modal and nonmodal behavior of the linear Hasegawa-Wakatani drift-wave model. Nonmodal behavior can play a role in this system because it is nonnormal, i.e. it does not have a complete set of orthogonal eigenvectors. The key parameter in the system is the adiabatic paramter C. For $C \gg 1$, the eigenvectors are complete and orthogonal with respect to the energy inner product; normal mode analysis gives a complete discription of the system. For $C = 0$, the system does not have a complete set of eigenvectors and the growth is nonmodal. For intermediate values of C we have shown that relative importance of the modal and nonmodal behavior is time-scale dependent. Our main conclusion is that for a given time-scale, there is a C_{crit} such that for $C < C_{crit}$ the behavior is nonmodal and for $C > C_{crit}$ the behavior is modal. Detailed results supporting this conclusion are the following.

- The pseudospectrum of the Hasegawa-Wakatani system shows that for small C, nonmodal growth is larger than the modal growth predicted by the spectrum; this nonmodal growth occurs at different wavenumbers than the maximum modal growth.

- For $C \ll 1$, drift-waves with $\beta_0 \approx 0$ have nonmodal growth rates comparable to the modal growth rates of the most unstable drift-waves ($C = 0.1$).

- The nonmodal behavior is generally a broad-spectrum phenomena. A consequence of this point is that ensemble averaged energy growth is greater for drift-waves with $C \ll 1$ than for drift-waves with $C \sim 1$ where narrow-spectrum modal behavior is dominant.

- Fluctuations that grow fastest initially only maintain string growth for $C = 10^{-5}$. Even for $C = 1$, the linear behavior on very short time scales ($t \ll 1$) differs from the normal mode analysis.

Appendix

We introduce new variables ψ_k defined by

$$\psi_k = M^{1/2} u_k, \tag{22}$$

where

$$M = \frac{1}{2} \begin{bmatrix} k^2 & 0 \\ 0 & 1 \end{bmatrix}. \tag{23}$$

The advantage of these variables is that $\|u\| = \|\psi\|_2$ where $\|\cdot\|$ is the energy norm and $\|\cdot\|_2$ is the usual root mean square norm, allowing the use of standard MATLAB routines to compute the various energy growth ratios. Equation (7) becomes

$$\frac{d}{dt} \psi_k = B \psi_k, \tag{24}$$

where

$$B = M^{1/2} A M^{-1/2}. \tag{25}$$

Note that A and B have the same eigenvalues and hence the same modal growth properties.

The energy growth ratios ξ and growth rates β are computed as follows. First,

$$\beta_0 = \max_{z \in \Lambda(B)} \operatorname{Re} z, \tag{26}$$

and $\xi_0(t) = e^{\beta_0 t}$. Then,

$$\xi_1(t) = \|e^{Bt}\|_2. \tag{27}$$

Then,

$$\xi_2(t) = \|e^{Bt} y\|_2, \tag{28}$$

where y is the *left* eigenvector of B whose eigenvalue has real part β_0 [5]. Then,

$$\xi_3(t) = \|e^{Bt} v\|_2, \tag{29}$$

where v is the leading right singular vector of $e^{B\tau}$ [35]. Then,

$$\xi_4(t) = \|e^{Bt} w\|_2, \tag{30}$$

where w is the leading eigenvector of $(B^\dagger + B)$ [4].

The growth rate ratio $\xi_5(t)$ is computing by considering an ensemble of initial conditions $\psi(0)$. In particular, suppose that the mean of the ensemble is zero

$$\langle \psi(0) \rangle = 0, \tag{31}$$

and that the covariance is given by

$$\langle \psi(0) \psi(0)^\dagger \rangle = Q, \tag{32}$$

where Q is the covariance matrix; $\langle \cdot \rangle$ denote average over initial conditions. Then, the ensemble averaged initial energy is

$$\langle \|\psi(0)\|_2^2 \rangle = \langle \operatorname{tr} \psi(0) \psi(0)^\dagger \rangle = \operatorname{tr} Q, \tag{33}$$

and the expected energy at time t is

$$\begin{aligned} \xi_5^2(t) &= \langle \|\psi(t)\|^2 \rangle = \langle \operatorname{tr} \psi(t) \psi(t)^\dagger \rangle \\ &= \langle \operatorname{tr} e^{Bt} \psi(0) \psi(0)^\dagger e^{B^\dagger t} \rangle = \operatorname{tr} e^{tB^\dagger} Q e^{Bt}. \end{aligned} \tag{34}$$

The simplest choice of Q and the one we use here is $Q = I/\operatorname{tr} I$, i.e. uncorrelated random initial conditions with expected unit initial energy.

References

[1] P. G. Drazin and W. H. Reid, *Hydrodynamic Stability* (Cambrigde University Press, Cambridge, 1981).

[2] J. Serrin, *Handbuch der Physik* (Springer-Verlag, Berlin, 1959), Vol. III/1.

[3] D. D. Joseph, *Stability of Fluid Motions* (Springer-Verlag, Berlin, 1976), Vol. I,II.

[4] L. N. Trefethen, A. E. Trefethen, and S. C. Reddy, Science **261**, 578 (1993).

[5] B. F. Farrell and P. Ioannou, J. Atmos. Sci. **53**, 2025 (1996).

[6] K. M. Butler and B. F. Farrell, Phys. Fluids A **4**, 1637 (1992).

[7] B. F. Farrell, J. Atmos. Sci. **42**, 163 (1988).

[8] R. Buizza and T. N. Palmer, J. Atmos. Sci. **52**, 1434 (1995).

[9] T. DelSole and B. F. Farrell, J. Atmos. Sci. **53**, 1781 (1996).

[10] S. C. Reddy, P. J. Schmid, and D. S. Henningson, SIAM J. Appl. Math **1**, 15 (1993).

[11] J. S. Baggett, T. A. Driscoll, and L. N. Trefethen, Phys. Fluids **7**, 833 (1995).

[12] B. F. Farrell and P. J. Ioannou, Phys. Fluids **8**, 1257 (1996).

[13] R. J. Goldston and P. H. Rutherford, *Introduction to Plasma Physics* (Institute of Physics Publishing, Bristol and Philadelphia, 1995).

[14] J. P. Freidberg, *Ideal Magnetohydrodynamics* (Plenum Press, New York, 1987).

[15] G. P. Galdi and S. Rionero, *Weighted Energy Methods in Fluid Dynamics and Elasticity, Lecture Notes Math.* (Springer Verlag, Berlin, 1985).

[16] H. Tasso and S. J. Camargo, N. Cimento B **107**, 733 (1992).

[17] D. Borba *et al.*, Phys. Plasmas **1**, 3151 (1994).

[18] G. D. Chagelishvili, A. D. Rogava, and D. Tsiklauri, Phys. Plasmas **4**, 1182 (1997).

[19] B. Scott, Plasma Phys. Control. Fusion **39**, 1635 (1997).

[20] A. Hasegawa and M. Wakatani, Phys. Rev. Lett. **50**, 682 (1985).

[21] M. Wakatani and A. Hasegawa, Phys. Fluids **27**, 611 (1984).

[22] S. J. Camargo, D. Biskamp, and B. D. Scott, Phys. Plasmas **2**, 48 (1995).

[23] D. Biskamp, S. J. Camargo, and B. D. Scott, Phys. Lett. A **186**, 239 (1994).

[24] A. E. Koniges, J. A. Crotinger, and P. H. Diamond, Phys. Fluids B **4**, 2685 (1992).

[25] D. Biskamp and A. Zeiler, Phys. Rev. Lett. **74**, 706 (1995).

[26] A. Zeiler, D. Biskamp, and J. F. Drake, Phys. Plasmas **3**, 3947 (1996).

[27] A. Hasegawa and K. Mima, Phys. Fluids **21**, 87 (1978).

[28] R. M. Castro *et al.*, Phys. Plasmas **3**, 971 (1996).

[29] P. R. Halmos, *A Hilbert Space Problem Book* (Van Nostrand-Reinhold, New York, 1967), 365 pp.

[30] L. N. Trefethen, SIAM Review **39**, 383 (1997).

[31] J. H. Wilkinson, *The Algebraic Eigenvalue Problem* (Clarendon Press, Oxford, England, 1965).

[32] B. F. Farrell, J. Atmos. Sci. **46**, 1193 (1989).

[33] Z. Toth and E. Kalnay, Bull. Amer. Meteor. Soc. **74**, 2317 (1993).

[34] F. Molteni, R. Buizza, T. N. Palmer, and T. Petroliagis, Q. J. R. Meteorol. Soc. **122**, 73 (1996).

[35] G. H. Golub and C. F. Van Loan, *Matrix Computations*, Third ed. (The Johns Hopkins University Press, Baltimore, 1996), 694 pp.